In Vivo Second-Harmonic Generation and *Ex Vivo* Coherent Anti-Stokes Raman Scattering Microscopy to Study the Effect of Obesity to Fibroblast Cell Function Using an Yb-Fiber Laser-Based CARS Extension Unit

DÓRA HALUSZKA,[1,2] KENDE LŐRINCZ,[1] GÁBOR MOLNÁR,[3] GÁBOR TAMÁS,[3] ATTILA KOLONICS,[2,4] RÓBERT SZIPŐCS,[2,4]* SAROLTA KÁRPÁTI,[1] AND NORBERT M. WIKONKÁL[1]

[1]*Department of Dermatology, Venereology and Dermatooncology, Semmelweis University Hungary, Budapest, Hungary*
[2]*Department of Applied and Nonlinear Optics, Institute for Solid State Physics and Optics, Budapest, Hungary*
[3]*MTA-SZTE Research Group for Cortical Microcircuits, Department of Physiology, Anatomy and Neuroscience, University of Szeged, Hungary*
[4]*R&D Ultrafast Lasers Ltd, Budapest, Hungary*

KEY WORDS obesity; skin; collagen; adipocyte; in vivo nonlinear microscopy; label-free imaging methods

ABSTRACT Nonlinear microscopy techniques are being increasingly used to perform *in vivo* studies in dermatology. These methods enable us to investigate the morphology and monitor the physiological process in the skin by the use of femtosecond lasers operating in the red, near-infrared spectral range (680–1,300 nm). In this work we used two different techniques that require no labeling: second harmonic generation (SHG) for collagen detection and coherent anti-Stokes Raman scattering (CARS) to assess lipid distribution in genetically obese murine skin. Obesity is one of the most serious public health problems due to its high and increasing prevalence and the associated risk of type 2 diabetes and cardiovascular diseases. Other than these diseases, nearly half of patients with diabetes mellitus suffer from dermatological complications such as delayed wound healing, foot ulcers and several other skin changes. In our experiment we investigated and followed the effects of obesity on dermal collagen alterations and adipocyte enlargement using a technique not reported in the literature so far. Our results indicate that the *in vivo* SHG and *ex vivo* CARS imaging technique might be an important tool for diagnosis of diabetes-related skin disorders in the near future. *Microsc. Res. Tech. 78:823–830, 2015*.

INTRODUCTION

The ability to follow the changes and distribution of various biological compounds in the skin is essential for better understanding the mechanism of diseases. Nonlinear microscopy offers a noninvasive, high-resolution and deeply penetrating optical imaging technique with high sensitivity (Denk et al., 1990). The epidermis and dermis both contain numerous endogenous chromophores, such as NADH, melanin, keratin, elastin, and collagen that can be visualized by various excitation wavelengths, without the need of exogenous contrast agents (Breunig et al., 2012). The combination of different modalities such as two-photon absorption fluorescence (TPAF), second harmonic generation (SHG) or coherent anti-Stokes Raman spectroscopy (CARS) are promising techniques to obtain detailed morphological and structural information about living tissue (Breunig et al., 2010; Han et al., 2005).

Obesity is defined as an excessive body fat accumulation that leads to various metabolic diseases, such as hypertension, cardiovascular disorders and type 2 diabetes (Kopelman, 2000). The most common diabetes-related skin lesions are impaired wound healing and foot ulcers (Reiber, 2002). In obesity, the subcutaneous adipose layer increases and adipocytes grow in size. It has been previously described that an increase of subcutaneous adipose layer has a suppressive effect on certain functions of fibroblasts that results in unfavorable changes in the structure of the dermis. This feedback may play an important role in the development of chronic diabetic skin complications, such as pressure ulcers (Ezure and Amano, 2011; Ezure et al., 2009). For this reason, there is a need to find a fast and

*Correspondence to: Róbert Szipőcs, Institute for Solid State Physics and Optics of Wigner RCP, Budapest, Hungary. E-mail: szipocs.robert@wigner.mta.hu

Received 16 January 2015; accepted in revised form 21 June 2015

REVIEW EDITOR: Alberto Diaspro

Conflict of Interest: AK and RS hold shares in R&D Ultrafast Lasers Ltd. Other authors declare no conflict of interest.

Author Contributions: DH prepared the samples for SHG and CARS images, DH, KA and RS recorded the microscope images, DH, KL evaluated the data, GM, GT and RS optimized the microscope and laser setup for CARS and SHG imaging, DH, KA, NW, SK and RS wrote the manuscript.

Contract grant sponsor: Hungarian Development Agency (NFÜ); Contract grant number: TECH-09-A2-2009-0134; Contract grant sponsor: Hungarian Brain Research Program; Contract grant number: KTIA_13_NAP-A-I/16; Contract grant sponsor: R&D Ultrafast Lasers Ltd.

DOI 10.1002/jemt.22545

Published online 24 July 2015 in Wiley Online Library (wileyonlinelibrary.com).

noninvasive diagnostic method that is able to detect these complications at an early stage.

The purpose of our work was to identify the main features and structural changes of diabetic murine skin. An additional aim was to develop a system that allows us to continuously monitor these changes. For this reason, we set out to use nonlinear microscopy (Bognar et al., 2014; Kolonics et al., 2014) for detection of the dermal collagen and subcutaneous adipocytes.

MATERIALS AND METHODS

Animals, Diet, and Methods

Identification of mutations in the *ob* gene has led to the discovery of leptin, which is the "satiety hormone." Its function is to regulate the energy balance by controlling the appetite in the central nervous system. Leptin receptors are primarily located in the hypothalamus; the hormone itself is produced and secreted by the adipocytes. The level of leptin secretion is directly proportional with the amount of fat stored in the adipose tissue: when the fat volume is increased, the high level of leptin suppresses the feeling of appetite in the brain. This establishes a direct connection between brain and fat tissue. In case of animals with an *ob* gene defects, leptin is not secreted in sufficient amount, leading to a lack of content, and uncontrolled food intake, a condition named hyperphagia. Genetically engineered leptin deficient mice gain weight rapidly and become obese, hyperinsulinemic and hyperglycemic. This makes them a valid model for metabolic syndrome, obesity and diabetes.

During our experiments we investigated three mouse groups. The 8-week-old female mice deficient for leptin (B6.V-Lep ob/ob) (Charles River, Italy) were divided into two groups, two mice per group, and were provided with two kinds of diet for 30 weeks. First ob/ob group received a normal diet (ob/ob—ND) having *ad libitum* access to food and water, while the second ob/ob group was kept on a calorie restricted diet (ob/ob—CRD) as described previously (Harrison et al., 1984). In the third group we used C57BL/6J mice (Charles River, Italy) with intact *ob* gene as controls (Control). Control mice were kept on *ad libitum* normal diet. Our experimental protocol was submitted to and approved by the Semmelweis University Animal Care and Use Committee. Body weight of each mouse was measured weekly. *In vivo* SHG imaging technique of the collagen was performed four times throughout the experimental period. Mice were anesthetized with 1.2% Avertin solution (0.23 mL/10 g, Sigma–Aldrich, Hungary) intraperitoneally then the fur was completely removed from the dorsal skin by shaving and plucking, prior to each measurement. They were laid in a custom designed mouse restrainer in order to ensure the precise positioning of the examined skin areas. A drop of distilled water, as a liquid contact medium, was spilled on the hairless dorsal skin and then covered with a glass slide. This glass covered dorsal skin area was placed under the microscope objective and measured multiple times. For each mouse, five z-stack images were recorded and analyzed.

Initially, we tried to *in vivo* visualize the adipocytes with the CARS imaging system, however, when we used the highest energy setting that safety considerations allowed us, the penetration depth of laser power was still not satisfactory. Proper optical representation requires an energy that causes thermal damages at the skin surface, so *in vivo* measurements were not performed in this setup. Instead, 4 mm full-thickness punch biopsies were taken, from identical dorsal locations, after the mice were euthanized. *Ex vivo* CARS imaging method was performed once at the end of the experiment on these specimens. Images were acquired in the direction of hypodermis to epidermis in order to improve image quality. The same e*x vivo* tissue specimens were fixed in formalin, embedded in paraffin and sections were stained with hematoxylin-eosin. Additionally, van Gieson staining was used to demonstrate changes in the collagen morphology. The dermal thickness and size of adipocytes were evaluated from van Gieson images using a Digimizer Image Analysis Software (Ostend, Belgium).

Because of the low number of mice in the three groups accurate statistical probes could not be used. For demonstration we compared the average values of the different groups regarding to body weigth, SHG intensities, dermal thickness and size of adipocytes.

Imaging Setup

Two- or multiphoton absorption autofluorescence (2PAF or MPAF) microscopy (Denk et al., 1990), second-harmonic generation (SHG) microscopy (Han et al., 2005), coherent anti-Stokes Raman scattering (CARS) (Evans and Xie, 2008) and stimulated Raman scattering (SRS) (Saar et al., 2010) allow label-free imaging of the tissue with chemical contrast and high spatial and temporal resolution. In 2PAF/MPAF and SHG imaging setups a single, typically tunable wavelenght, mode-locked laser is used for excitation of the sample. This is in contrast to CARS imaging systems, where two laser beams at two different frequencies, called the pump ω_p, and Stokes ω_S, are used to illuminate the sample. When the difference frequency between the two beams is tuned to match an intrinsic molecular vibrational frequency in the sample Ω_{vib}, a nonlinear interaction occurs: new light is generated at the anti-Stokes frequency, $\omega_{aS} = 2\omega_p - \omega_S$, by the CARS process. This process offers proper chemical selectivity, high spatial resolution, and video-rate imaging speeds *in vivo* in living animals and humans.

For single wavelength nonlinear microscopy, broadly tunable, femtosecond pulse Ti:sapphire lasers (Mayer et al., 1997) are typically used. However, recent years brought revolutionary progress in development of femtosecond pulse, all-fiber laser oscillators (Fekete et al., 2009) and amplifiers being suitable for nonlinear microscopy. For instance, a novel all-fiber, multimodal (2PAF + SHG + CARS) microscope system has been presented (Pegoraro et al., 2009). Fiber lasers are also interest because of the ease with which they can be combined with endoscopy (Saar et al., 2011), which would greatly increase the utility of CARS micrscopy for preclinical applications and tissue imaging.

Currently there is a large number of 2PAF microscope systems all around the world, in which broadly tunable Ti:sapphire lasers are used as a single wavelength, tunable pulsed laser source. However, after a relatively simple, cost efficient modification/upgrade of the 2PAF laser and microscope setups, one can make his system capable for CARS microscopy as well.

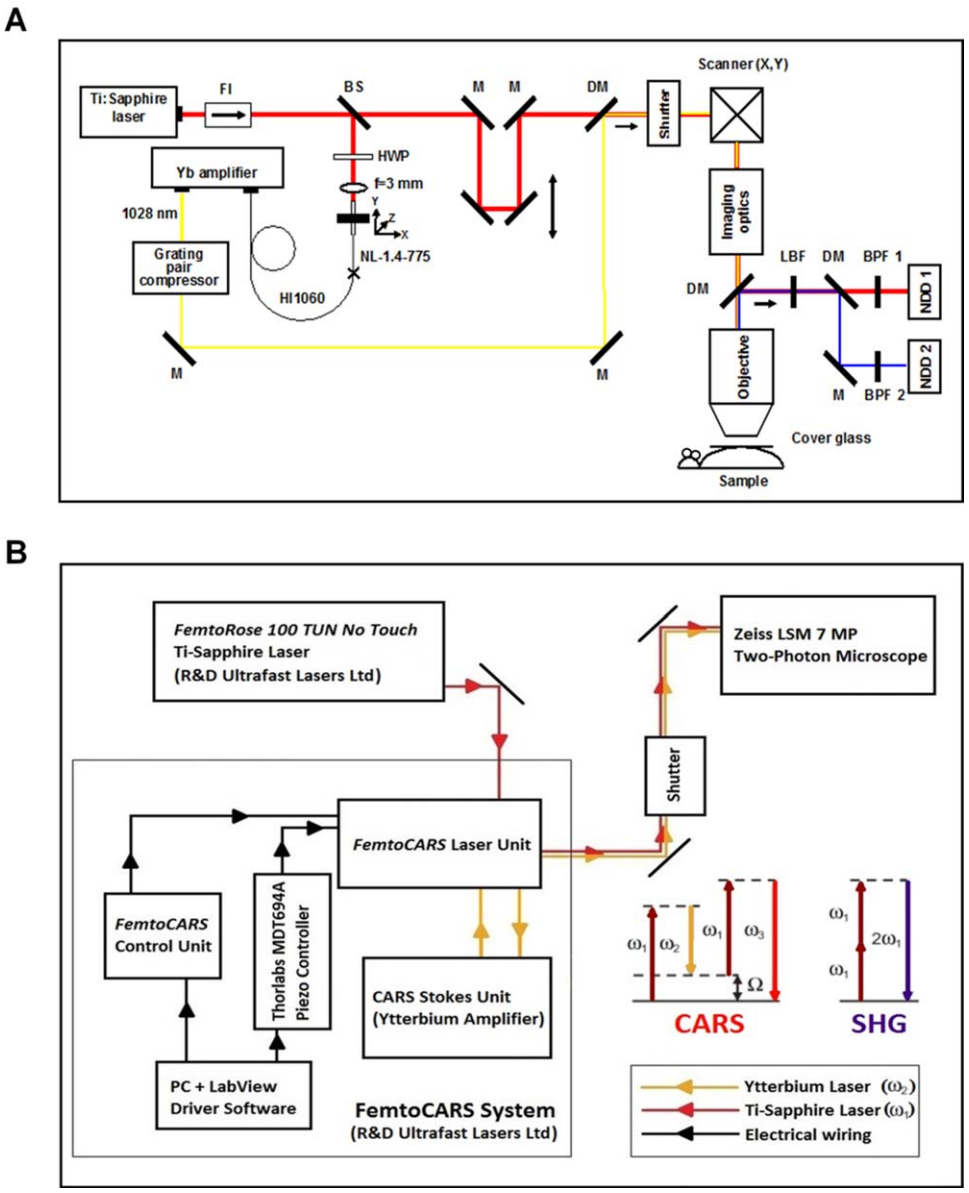

Fig. 1. Experimental setup used for SHG/CARS imaging. **A**: Detailed description of the SHG/CARS upgrade for our standard LSM 7MP (Carl Zeiss) 2PAF microscope (including additional bulk and fiber optics, Yb-fiber laser amplifier and optical filters); FI: Faraday-isolator, BS: beam splitter, HWP: half wave plate, NL-1.4-775: photonic crystal fiber, HI-1060: single-mode fiber, M: (broadband) beam stearing mirrors, DM: dichroic mirror, LBF: laser blocking filter, BPF: band-pass filter, NDD: non-descanned detector. Position of the examined mice during *in vivo* imaging is also shown in the figure. **B**: Block scheme of the whole SHG/CARS imaging system including main system components, beam paths and electrical wiring. Inset: Energy diagrams corresponding to the CARS and SHG processes: ω_1 ($=\omega_p$)—the frequency of Ti:sapphire laser (pump), ω_2 ($=\omega_S$)—the frequency of Yb-amplifier (Stokes), ω_3 ($=\omega_{as}$)—the frequency of light generated during the CARS process, Ω ($=\Omega_{vib}$) – vibration frequency of the investigated molecule. [Color figure can be viewed in the online issue, which is available at wileyonlinelibrary.com.]

In this section we briefly introduce our relatively simple, cost efficient, fiber laser based CARS extension unit, which can be adopted for most of the femtosecond pulse, tunable Ti:sapphire lasers used for 2PAF imaging (Kolonics et al., 2012) (Fig. 1). We will also discuss later minor modifications that were required for our SHG imaging.

A detailed description of the SHG/CARS upgrade for our standard 2PAF microscope, which includes additional bulk and fiber optics, a two-stage Yb-fiber laser amplifier and new optical filters placed into the microscope, is show in Figure 1A. A broadly tunable, femtosecond pulse Ti:sapphire laser generates nearly transform limited, $\tau_{FWHM} \sim 190$ fs pulses at a central wavelength of 796 nm. A Faraday isolator (FI) placed in the beam path assures that there is no back reflection to the laser oscillator from the different optical elements, such as the optical fiber ends, that might perturb mode-locking performance. An achromatic beam-splitter (BS) divides the laser power into two

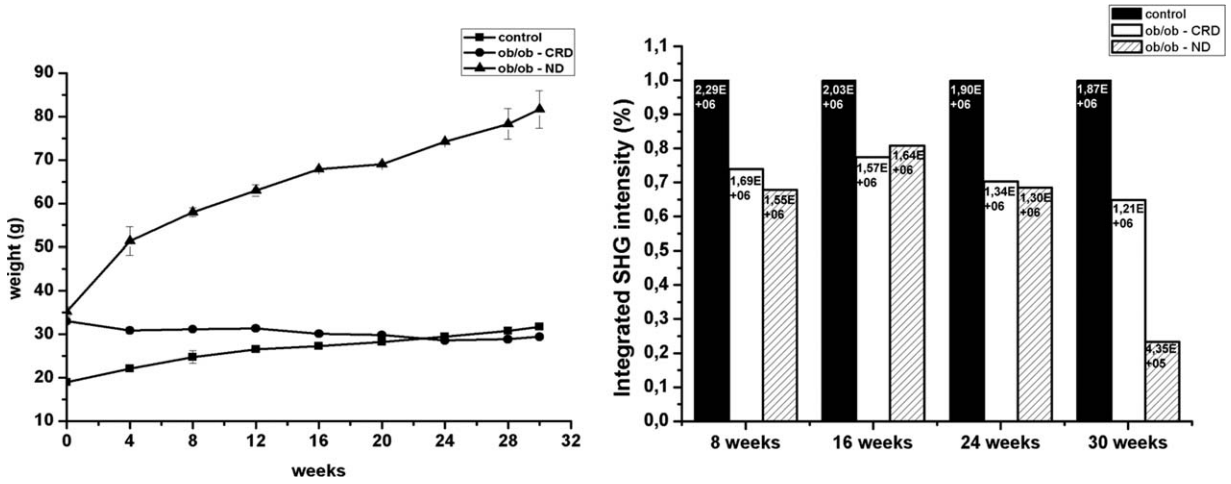

Fig. 2. Results of body weight changes and SHG intensity of dermal collagen measured and followed-up for 30 weeks. **A**: Increase of body weight in groups of mice during 30 weeks. At the beginning of the experiments (week 0) animals in various diet groups were already different; animals with leptin deficiency had higher body weight compared to controls. At week 8 the body weight increase of ob/ob—ND group was approximately twofold higher compared to other groups. The body weight of ob/ob—CRD group stayed relatively constant from week 8. Error bars represent standard deviation (SD) **B**: SHG intensity levels measured after 8, 16, 24, and 30 weeks. Results are normalized to values referring to the control group. Numbers on the top of the bars represent the measured and averaged SHG intensity values without normalization. We could not observe significant changes in SHG intensity among mice groups for nearly 30 weeks. At the final measuring timepoint at week 30, however, the skin of mice in the ob/ob—ND group had a remarkably lower SHG intensity compared to control and ob/ob—CRD mice. Also, a similar change was seen when the week 30 values were compared to the initial values.

parts: the reflected beam is focused into a small core area photonic crystal fiber (NL-1.4-775, NKT Photonics, Denmark) by a high NA, achromatic focusing lens, which generates the seed pulses for the two-stage Yb-amplifier unit operating at 1,028 nm. The transmitted beam, which plays the role of tunable pump beam for CARS measurements, directly goes into the nonlinear micrscope passing through a precision delay stage, which assures the zero delay difference between the tunable pump and amplified, compressed Stokes pulses. The pump and Stokes pulses are inherently synchronized, since the relatively broadband seed pulses of the amplifier are generated by the Ti:sapphire laser pulses by efficient nonlinear wavelenght conversion in a ~100 mm long photonic crystal fiber (PCF). After the two-stage Yb-amplifier, we obtain optical pulses having a central wavelenght of ~1,028 nm and a FWHM bandwidth of ~10 nm. A transmission grating pair compressor is used for temporal compression of the Stokes pulses, which is required for optimization of the CARS signal. The ~796 nm pump pulses and the ~1,028 nm Stokes pulses are combined by a dichroic mirror (DM) before entering the scanning microscope.

The SHG signal of collagen and the CARS signal of adipocytes are efficiently separated between the two NDD detectors by a long-pass dichroic beamsplitter (LP555). The signal to noise ratio is improved by narrowband ($\Delta\lambda \sim 10$ nm) bandpass filters respectively centered at around the SHG signal wavelenght for collagen ($\lambda \sim 398$ nm) and the anti-Stokes signal wavelenght of adipocytes ($\lambda \sim 649$ nm), which corresponds to the CH_2 symmetric streching vibration resonance of saturated fatty acids in our setup. The average powers of the two laser beams measured at the sample surface were ~20 and ~10 mW for the Ti:sapphire laser and the Yb-amplifiers, respectively. The 3D images were obtained by computer controlled precise positioning of the objective along the z-axis ("z-stack images"), which enabled us to image the samples at different tissue depths. Generally, the maximum imaging depth was ~60 μm with imaging intervals of 5 μm. The image resolution and speed were chosen at 1,024 pixels with 12.61 μsec pixel dwell time respectively. The laser beams were focused by a 20×, water immersion objective (W-Plan – APOCHROMAT 20x/1,0 DIC (UV) VIS-IR, Carl Zeiss, Germany), which resulted in an $\sim 0.6 \times 0.6$ mm^2 imaging area. Using a 12.61 μs pixel dwell time and the average power values listed above we could not observe any thermal damage of the samples during our measurements. The 3D images were captured by the commercial ZEN software of the LSM 7MP microscope (Carl Zeiss, Germany).

Block scheme of the whole SHG/CARS imaging system that was used for our SHG/CARS measurements is shown in Figure 1B. It includes main system components, beam paths and electrical wiring. In the inset, energy diagrams corresponding to the CARS and SHG processes are shown.

The 3D SHG/CARS images were taken by a commercial Axio Examiner LSM 7 MP laser scanning 2P microscope (Carl Zeiss, Germany) after the minor modifications discussed above. A broadly tunable, femtosecond pulse Ti:sapphire laser (*FemtoRose 100 TUN NoTouch*) is used for SHG imaging of collagen. It is also used as a pump beam of the CARS measurements. An inherently synchronized, two-stage Yb-fiber amplifier (*CARS Stokes Unit*) generates the Stokes pulses for CARS imaging of adipocytes. Synchronization (i.e., temporal overlapping) and spatial overlapping of the pump and the Stokes beam is assured by a *Femto-CARS Laser Unit*, which has the following functions: (i) it generates the seed pulses for the two-stage Ytterbium amplifier, (ii) it compresses the amplified Stokes

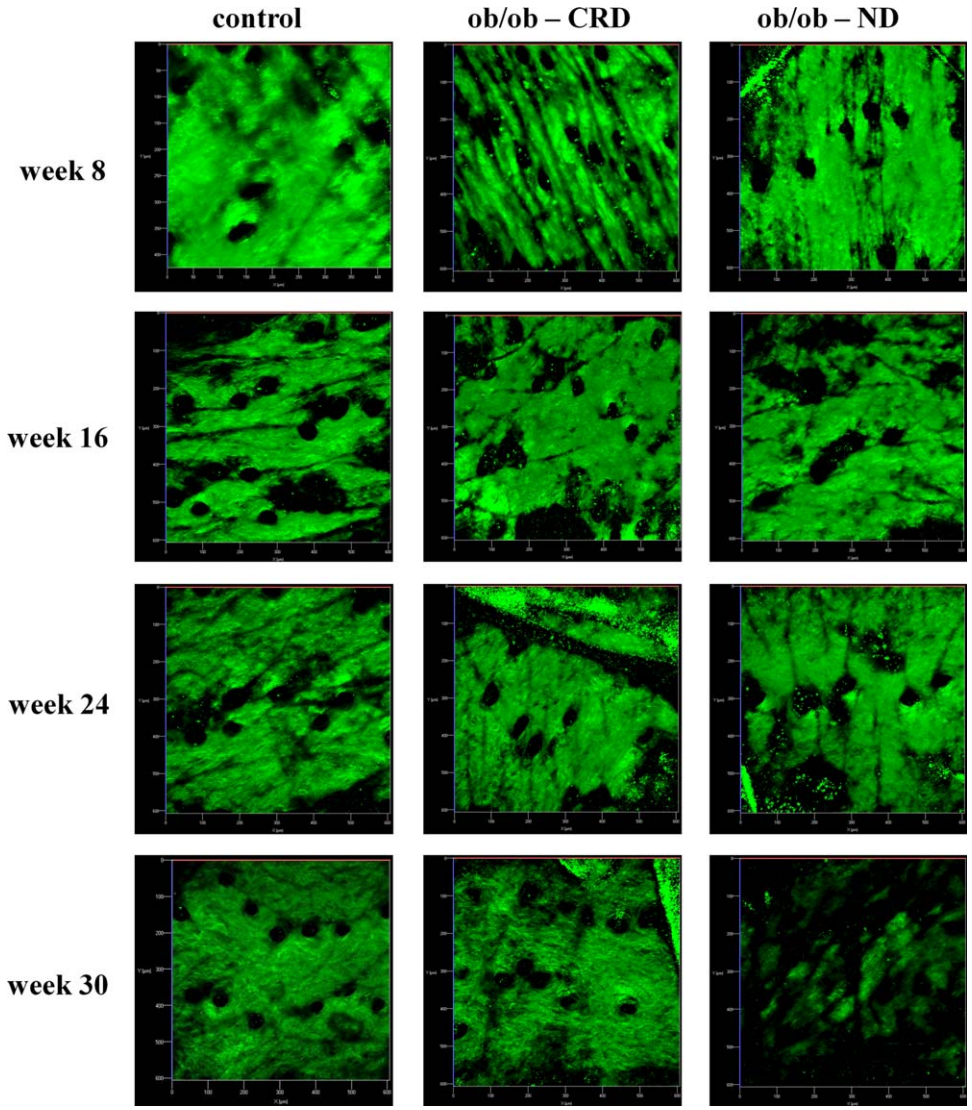

Fig. 3. The 3D-SHG images of dermal skin of mice in various diet groups. Dermal collagen degradation in ob/ob—ND mice was clearly visible at week 30. The images were projected in the z-direction and were recorded starting from stratum corneum ($z = 0$ μm) to the deeper layers of dermis ($z = 60$ μm) using a 796 nm laser excitation wavelength. Imaging area is $\sim 0.6 \times 0.6$ mm^2. [Color figure can be viewed in the online issue, which is available at wileyonlinelibrary.com.]

pulses, (iii) using a precision delay stage with step motor and piezo control, it assures the zero delay difference between the tunable pump and fixed wavelength Stokes pulses, (iv) using a half-wave plate, polarization of the pump and the Stokes beams are matched here for a maximum CARS signal, and finally (v) it combines and transmits the pump and the Stokes beams to the scanning SHG/CARS microscope.

RESULTS

Body Weight of Mice

The ob/ob knockout group kept on a standard diet (ob/ob-ND) for 30 weeks had a notably higher body weight (63.65 ± 4.31 g) than the control (26.63 ± 4.12 g) and the calorie restricted groups (30.33 ± 1.39 g). At the end of the study, the weight gain in the ob/ob group was three times higher than in the other groups (see in Figure 2A).

Changes in Collagen Morphology

During the first three measuring session, at weeks 8, 16, and 24, we could not observe significant differences in the SHG intensities among the groups using the same laser and microscope parameters. It was noted, however, that the ob/ob—ND and ob/ob—CRD groups had lower SHG intensity in each measuring time compared to the control group. At the final evaluation time, at week 30, when the ob/ob—ND group had almost tripled its body weight, the SHG intensity decreased remarkably when compared to the controls (Fig. 2B). The collagen morphology in the ob/ob—CRD group was normal and fiber-rich, as was in the control

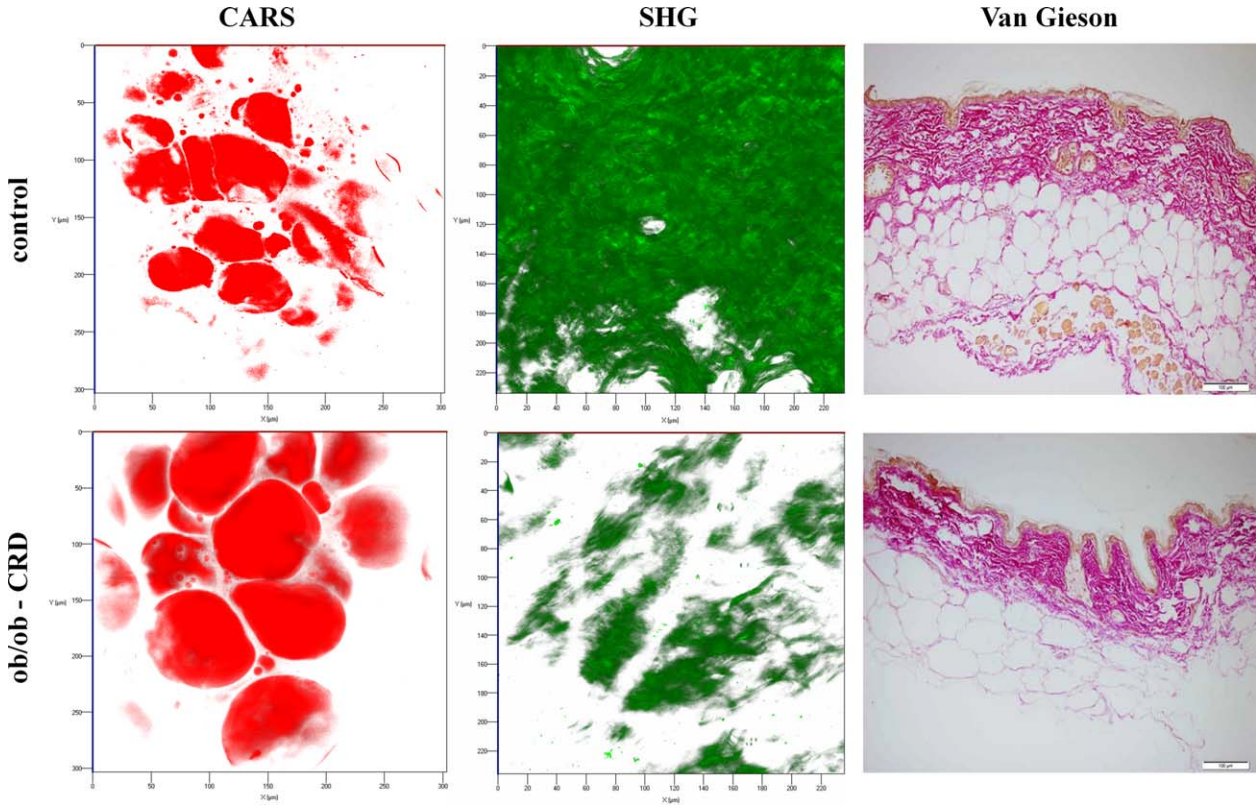

Fig. 4. Comparison of adipocyte sizes by CARS measurement and the collagen morphology, determined by SHG, and *ex vivo* van Gieson staining of control and ob/ob—ND groups. The 3D CARS and SHG images are projected in *z*-direction and imaging area is ~0.6 × 0.6 mm^2. The enlarged adipocytes, damaged collagen fibers and thinner dermis in case of leptin deficient mice are clearly visible, in contrast to control group. [Color figure can be viewed in the online issue, which is available at wileyonlinelibrary.com.]

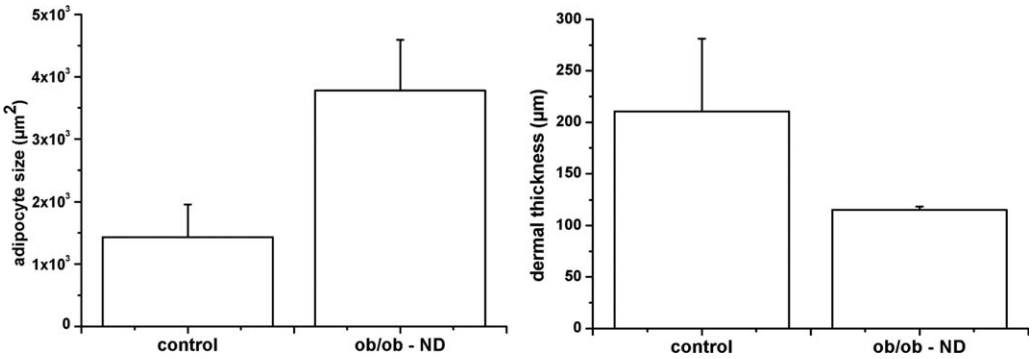

Fig. 5. Graphs show the dermal thickness and adipocyte sizes in the skin of mice in the control and ob/ob—ND groups. Digital images of van Gieson stained sections were evaluated at the end of study by using Digimizer Image Analysis software. The bars represent the mean values of thicknesses and adipocyte sizes of the control and ob/ob-ND groups. Error bars represent standard deviation (SD).

animals (Fig. 3). The ob/ob—ND group displayed reduced dermal collagen content and the SHG intensity anti-correlated with the degree of obesity.

Adipocyte Morphology Changes

The subcutaneous adipocytes in the ob/ob—ND group were considerably larger (3678.06 ± 984.95 μm^2) compared to the control group (1429.1 ± 316.25 μm^2). Furthermore, along with the enlarged adipocytes in the ob/ob—ND group, the dermal thickness decreased greatly (115.2 ± 27.35 μm) compared to control group (210.42 ± 8.4 μm) as shown in Figures 4 and 5.

DISCUSSION

Obesity and type 2 diabetes represent one of the most serious public health problem and their worldwide epidemic is reaching an alarming rate (Rosen and Spiegelman, 2014). In the case of diabetes mellitus, almost half

of the patients suffer from dermatological complications. The biophysical background of these diseases comprises of altered metabolic conditions, circulational, innervational and immunological disorders.

Therefore it is crucial to find fast and noninvasive imaging methods that are able to identify these skin lesions in early stages. The most popular microscopy techniques are based on various nonlinear optical effects such as two-photon excited fluorescence, second harmonic generation or fluorescence life-time imaging (FLIM), which are able to monitor the physiological processes in the skin (Bennassar et al., 2013; Koehler et al., 2011; Seidenari et al., 2012; Tanaka et al., 2013). Lipids, however, are intrinsically non-fluorescent and difficult to tag with fluorophores, thus, the efficacy of use of fluorescence-based imaging methods is limited. To better understand the regulation and biology of obesity, new imaging techniques are required. In recent years the use of coherent anti-Stokes Raman scattering and stimulated Raman scattering microscopy techniques have become increasingly popular. These tools permit us to visualize a broad range of biological samples such as lipid bilayers, lipid droplets, neuronal myelin sheats, DNA, proteins and small metabolits *in vivo* without any labeling (Freudiger et al., 2008; Jungst et al., 2013).

In this work we demonstrated that one can identify all major features and changes of diabetic skin in ob/ob knockout mice using *in vivo* SHG and *ex vivo* CARS imaging modalities. This imaging modality was able to show a negative correlation between body weight and SHG-intensity of the dermal collagen, as well as between the size of adipocytes and dermal thickness. However, we could not observe such dramatic effects in the case of calorie-restricted leptin deficient group. These results suggest that it is not the genotype that is responsible for changes in the dermal collagen but metabolic conditions play a determinant role. One invaluable advantage of SHG z-stack imaging technique is that it can be done *in vivo*, without sacrificing the animals. This is an indicator that this technique could be safely used in human diagnostics as well. Furthermore we compared the *in vivo* SHG collagen images with the corresponding *ex vivo* van Gieson stained images. We can conclude that the SHG imaging technique is more sensitive for the detection of structural alterations and fragmentation of dermal collagen when compared to the histological analysis performed on van Gieson stained sections. We can say that the noninvasive SHG technique presented is suitable for accurate visualization of early changes in the collagen structure *in vivo*. The biomechanical properties of dermal collagen and skin elasticity are crucial in obese patients. The impaired dermal functions such as reduced synthesis and degradation of extracellular matrix proteins contribute to the development of severe connective tissue alterations leading to diabetes related skin lesions (Ezure and Amano, 2011) or even make the person susceptible for deep soft tissue infections. Physical exercise is an effective therapy to treat many components of metabolic syndrome such as obesity, hypertension or insufficient cardiac function (Schjerve et al., 2008). Several studies examined the positive effects of exercise in obesity related complications recently. One must note, however, that a serious limitation of these works was that young adult animals have been used (Schjerve et al., 2008), whereas metabolic syndrome usually occurs in the elderly.

Our belief is that fluorescent label-free *in vivo* nonlinear microscopy, which includes two-photon excited fluorescence (TPEF), second- or third-harmonic generation (SHG, THG), fluorescence life-time imaging (FLIM) or Coherent anti-Stokes Raman Scattering (CARS) technique, is a versatile tool for skin research and for the esthetic industry. The CARS technique presented here can be used for *in vivo* label-free 3D visualization of lipid bilayers, lipid droplets, neuronal myelin sheets and small metabolites for instance without any labeling. Existing limitations on the imaging depth of the CARS system presented can be overcome by using lower repetition rate laser sources (Antal and Szipocs, 2012), longer excitation laser wavelengths and/or THG imaging method of lipids (Liao et al., 2013), which can pave the way for *in vivo* diagnostics of obesity related structural changes of the skin.

In summary, we were able to demonstrate the usability of nonlinear imaging techniques, SHG and CARS, in our experimental setting. This made possible an *in vivo* evaluation of the main structural alterations in the skin of genetically obese mice. Further, for the first time in the literature, we were able to follow and compare these processes in groups of mice kept on restricted or unlimited diet. With these measurements we were able to show that diet is more important than genetic predisposition in obesity-related skin deterioration. Our results prove and highlight the importance of body weight control and emphasize that with the use of proper diagnostic tool skin related complications could be detected at an early stage.

REFERENCES

Antal PG, Szipocs R. 2012. Tuneable, low-repetition-rate, cost-efficient femtosecond Ti: Sapphire laser for nonlinear microscopy. Appl Phys B 107:17–22.

Bennassar A, Carrera C, Puig S, Vilalta A, Malvehy J. 2013. Fast evaluation of 69 basal cell carcinomas with ex vivo fluorescence confocal microscopy: Criteria description, histopathological correlation, and interobserver agreement. JAMA Dermatol 149:839–847.

Bognar P, Nemeth I, Mayer B, Haluszka D, Wikonkal N, Ostorhazi E, John S, Paulsson M, Smyth N, Pasztoi M, Buzas EI, Szipocs R, Kolonics A, Temesvari E, Karpati S. 2014. Reduced inflammatory threshold indicates skin barrier defect in transglutaminase 3 knockout mice. J Invest Dermatol 134:105–111.

Breunig HG, Buckle R, Kellner-Hofer M, Weinigel M, Lademann J, Sterry W, Konig K. 2012. Combined in vivo multiphoton and CARS imaging of healthy and disease-affected human skin. Microsc Res Tech 75:492–498.

Breunig HG, Studier H, Konig K. 2010. Multiphoton excitation characteristics of cellular fluorophores of human skin in vivo. Opt Express 18:7857–7871.

Denk W, Strickler JH, Webb WW. 1990. Two-photon laser scanning fluorescence microscopy. Science 248:73–76.

Evans CL, Xie XS. 2008. Coherent anti-stokes Raman scattering microscopy: Chemical imaging for biology and medicine. Annu Rev Anal Chem 1:883–909.

Ezure T, Amano S. 2011. Negative regulation of dermal fibroblasts by enlarged adipocytes through release of free fatty acids. J Invest Dermatol 131:2004–2009.

Ezure T, Hosoi J, Amano S, Tsuchiya T. 2009. Sagging of the cheek is related to skin elasticity, fat mass and mimetic muscle function. Skin Res Technol 15:299–305.

Fekete J, Cserteg A, Szipocs R. 2009. All-fiber, all-normal dispersion ytterbium ring oscillator. Laser Phys Lett 22:49–53.

Freudiger CW, Min W, Saar BG, Lu S, Holtom GR, He C, Tsai JC, Kang JX, Xie XS. 2008. Label-free biomedical imaging with high

sensitivity by stimulated Raman scattering microscopy. Science 322:1857–1861.
Han M, Giese G, Bille J. 2005. Second harmonic generation imaging of collagen fibrils in cornea and sclera. Opt Express 13:5791–5797.
Harrison DE, Archer JR, Astle CM. 1984. Effects of food restriction on aging: Separation of food intake and adiposity. Proc Natl Acad Sci USA 81:1835–1838.
Jungst C, Klein M, Zumbusch A. 2013. Long-term live cell microscopy studies of lipid droplet fusion dynamics in adipocytes. J Lipid Res 54:3419–3429.
Koehler MJ, Speicher M, Lange-Asschenfeldt S, Stockfleth E, Metz S, Elsner P, Kaatz M, Konig K. 2011. Clinical application of multiphoton tomography in combination with confocal laser scanning microscopy for in vivo evaluation of skin diseases. Exp Dermatol 20:589–594.
Kolonics A, Csáti D, Antal PG, Szipőcs R. 2012. A simple, cost efficient fiber amplifier wavelength extension unit for broadly tunable, femtosecond pulse Ti-sapphire lasers for CARS microscopy. Biomedical Optics and 3D Imaging, OSA Technical Digest (Optical Society of America), paper BSu3A.28.
Kolonics A, Csiszovszki Z, Toke ER, Lorincz O, Haluszka D, Szipocs R. 2014. In vivo study of targeted nanomedicine delivery into Langerhans cells by multiphoton laser scanning microscopy. Exp Dermatol 23:596–605.
Kopelman PG. 2000. Obesity as a medical problem. Nature 404:635–643.
Liao YH, Chen SY, Chou SY, Wang PH, Tsai MR, Sun CK. 2013. Determination of chronological aging parameters in epidermal keratinocytes by in vivo harmonic generation microscopy. Biomed Opt Express 4:77–88.
Mayer EJ, Mobius J, Euteneuer A, Ruhle WW, Szipocs R. 1997. Ultrabroadband chirped mirrors for femtosecond lasers. Opt Lett 22: 528–530.
Pegoraro AF, Ridsdale A, Moffatt DJ, Pezacki JP, Thomas BK, Fu L, Dong L, Fermann ME, Stolow A. 2009. All-fiber CARS microscopy of live cells. Opt Express 17:20700–20706.
Reiber GE. 2002. Epidemiology of diabetic foot ulcers and amputation: Evidence for prevention. The evidence base for diabetes care. Chichester, UK: Wiley. pp. 641–665.
Rosen ED, Spiegelman BM. 2014. What we talk about when we talk about fat. Cell 156:20–44.
Saar BG, Freudiger CW, Reichman J, Stanley CM, Holtom GR, Xie XS. 2010. Video-rate molecular imaging in vivo with stimulated Raman scattering. Science 330:1368–1370.
Saar BG, Johnston RS, Freudiger CW, Xie XS, Seibel EJ. 2011. Coherent Raman scanning fiber endoscopy. Opt Lett 36:2396–2398.
Schjerve IE, Tyldum GA, Tjonna AE, Stolen T, Loennechen JP, Hansen HE, Haram PM, Heinrich G, Bye A, Najjar SM, Smith GL, Slordahl SA, Kemi OJ, Wisloff U. 2008. Both aerobic endurance and strength training programmes improve cardiovascular health in obese adults. Clin Sci (Lond) 115:283–293.
Seidenari S, Arginelli F, Dunsby C, French P, Konig K, Magnoni C, Manfredini M, Talbot C, Ponti G. 2012. Multiphoton laser tomography and fluorescence lifetime imaging of basal cell carcinoma: morphologic features for non-invasive diagnostics. Exp Dermatol 21: 831–836.
Tanaka R, Fukushima S, Sasaki K, Tanaka Y, Murota H, Matsumoto T, Araki T, Yasui T. 2013. In vivo visualization of dermal collagen fiber in skin burn by collagen-sensitive second-harmonic-generation microscopy. J Biomed Opt 18:61231.